JMEPEG (2021) 30:7730–7740
https://doi.org/10.1007/s11665-021-05964-1

1059-9495/$19.00

Microstructure, Tensile Properties, and Wear Resistance of In Situ TiB_2/6061 Composites Prepared by High Energy Ball Milling and Stir Casting

Weibin Zhuang, Hairui Yang, Weibo Yang, Jialong Cui, Liguo Huang, Chun Wu, Jingfu Liu, Yuejun Sun, and Chao Meng

Submitted: 8 November 2020 / Revised: 14 May 2021 / Accepted: 16 May 2021 / Published online: 26 July 2021

In-situ synthesized TiB_2/6061 composites were prepared from Al-K_2TiF_6-KBF_4 by high energy ball milling and stir casting. Phase analysis and microstructure observation of the samples were characterized by XRD, SEM and EDS, respectively. The effect of TiB_2 particle content on the microstructure, tensile properties and wear resistance of the composites was studied. The results show that the average size of TiB_2 particles is 1 μm, which is polygonal shape. The average grain size of the composites can be refined significantly as the TiB_2 particle mass content increased from 1 to 3%; however, the grain coarsening occurs in the 5 wt.% TiB_2/6061composites. The 3 wt.% TiB_2/6061 composites have best tensile strength, yield strength and Young's modulus among the composites in ranges of the TiB_2 mass fraction from 1 to 5%. Strengthening mechanisms of the TiB_2/6061 composites were fine grain strengthening, Orwan strengthening and CTE strengthening, in which the CTE strengthening plays an important role as increasing the TiB_2 content. The pin-on-disk wear test results indicated that the average friction coefficient and wear rate of the TiB_2/6061 composites increased firstly and then decreased with increasing the TiB_2 content from 1 to 5 wt.%. The wear mechanism of the TiB_2/6061 composites was discussed.

Keywords aluminum matrix composites, in-situ synthesized, microstructure, strengthening mechanisms, TiB_2 particles

1. Introduction

Compared with the traditional aluminum alloy, particle reinforced aluminum matrix composites (AMCs) have the advantages of high strength, high stiffness, high toughness, high wear resistance and good fatigue resistance (Ref 1-4). Therefore, particle reinforced AMCs have broad application prospects in aerospace, automotive and electronic fields (Ref 5-9).

At present, the preparation methods of particles reinforced AMCs mainly include the additive method and the in-situ method (Ref 10-13). Compared with the additive method, in-situ particles reinforced AMCs have received extensive attention from researchers in recent years due to their simple preparation process, good bonding between the reinforcement and the matrix, and the excellent properties of the composites (Ref 14-15). 2xxx, 6xxx, and 7xxx series aluminum alloys are commonly used as the matrix of AMCs (Ref 2, 5, 7, 10). Among them, 6061 aluminum alloys have generated significant interest as their outstanding properties (Ref 16-18). The ceramic particles such as TiB_2, TiC and Al_2O_3 are usually used as the in-situ formed phase to fabricate the AMCs (Ref 17-21). TiB_2 particles have high hardness, high melting point, good electrical and thermal conductivity, and are regarded as a very ideal reinforcement for AMCs (Ref 22-26).

In previous literatures, TiB_2 particles reinforced AMCs were synthesized by the chemical reactions of Al-K_2TiF_6-KBF_4 (Ref 24-26), Al-TiO_2-B_2O_3 (Ref 27, 28) and Al-Ti-B (Ref 17, 29). The flux-assisted synthesis, using the Al-K_2TiF_6-KBF_4 reaction system, is originated from a LSM method by P. Davies and co-workers in the 1990s (Ref 30). Owing to its low cost and easy control of the reinforcement content, the flux-assisted synthesis is the most popular method to prepare in-situ synthesized TiB_2 particles reinforced AMCs. Liu et al. fabricated in-situ TiB_2/Al composites at 900 °C and the grain size of the matrix refined significantly by the TiB_2 particles (Ref 24). Mozammil et al. prepared in-situ TiB_2/Al composites at 780 °C by using the flux-assisted synthesis and the size of TiB_2 particles was smaller than 2 μm (Ref 25). Chen et al. processed TiB_2/Al composites at 860 °C and the size of in-situ synthesized TiB_2 particles was in the range of 0.1∼2 μm (Ref 26). Al_3Ti phase was generated during the composites processing in those researches. Tee et al. reported that Al_3Ti phase can decrease the yield of TiB_2/Al composites (Ref 29). In order to obtain the in-situ particulate reinforced AMCs with excellent properties, the formation of Al_3Ti phase should be avoided during the processing. The formation of Al_3Ti in Al-TiO_2-B_2O_3 reaction system can be effectively inhibited under the starting materials ball milling condition (Ref 27).

In the present paper, in-situ synthesized TiB_2/6061 composites were prepared from Al-K_2TiF_6-KBF_4 by high energy ball milling combined with stir casting technology. The phase

Weibin Zhuang and Hairui Yang contributed equally to this work.

Weibin Zhuang, Jialong Cui, Liguo Huang, Chun Wu, Jingfu Liu, Yuejun Sun, and **Chao Meng**, School of Materials Science and Engineering, Liaoning Technical University, Fuxin, China; **Hairui Yang**, School of Materials Science and Engineering, Liaoning Technical University, Fuxin, China; and Avic Chengdu CAIC Electronics Co., LTD, Chengdu, China; and **Weibo Yang**, China Building Materials Test and Certification Group Co., LTD., Beijing, China. Contact e-mail: mengchao_ja@yeah.net.

analysis and microstructure of the composites were investigated. The effect of TiB_2 particle content on the microstructure, tensile properties and wear resistance of the composites was studied. Strengthening mechanism and wear mechanism were discussed.

2. Experimental

2.1 Materials

6061 aluminum alloy was selected as the matrix of the composites, and its nominal chemical composition is 98 wt.% Al, 0.4∼0.8 wt.% Si, 0.15∼0.4 wt.% Cu, 0.15 wt.% Mn, 0.8∼1.2 wt.% Mg, 0.25 wt.% Zn, 0.15 wt.% Ti and 0.7 wt.% Fe. Commercial available Al powder, K_2TiF_6 powder and KBF_4 powder, both of which have a purity of 98%, are used as the starting materials for preparing the reinforcement.

2.2 Preparation of the Composites

Al powder with an average particle size 20 μm, K_2TiF_6 with an average particle size 150 μm and KBF_4 powder with an average particle size 60 μm were weighed separately according to the mole ratio of Ti: B = 1:2 and the mass ratio of Al: (Ti + B)=1:1. The mixed powder was mixed by a planetary ball mill machine with ZrO_2 ball-to-powder weight ratio of 10:1 and milled at 300 rpm/min for 10 h. The diameter of ZrO_2 balls is 8 mm. The SEM comparison of the powders before and after ball milling is shown in Fig. 1. For each experiment, 1 kg 6061 aluminum alloy was melted and heated to 845 °C in a graphite crucible under argon atmosphere, using a resistance furnace. The schematic illustration of set-up for preparing in-situ TiB_2/6061 composites is shown in Fig. 2. The graphite crucible shown in Fig. 2 has a capacity of melting 2 kg aluminum alloy. A number of aluminum foil wrapped preforms with a size of 20 × 20 mm were pressed into melt 6061 aluminum alloy according to the in-situ synthesized nominal mass fraction of 1 , 3, 5 wt.% TiB_2 in the composites. The mechanical stirring was applied to the melt at the speed of 150 rpm/min for 30 min. Then, the molten material was cooled to 720 °C for refining, slag stripping and degassing. As the molten material temperature decreased to 700 °C, the molten material was poured into the pre-heated (300 °C) graphite mold (70 × 130 × 30 mm), and in-situ synthesized TiB_2/6061 composites can be obtained; the process flow is shown in Fig. 3.

2.3 Experimental Method

The differential scanning calorimetry (DSC) analysis of the mixed powder was carried by a CRY-2P high temperature differential thermal analyzer under nitrogen atmosphere from 20 to 1150 °C at a heating rate of 20 °C/min. Phase identification of the samples was conducted using the Shimadzu XRD-6100 X-ray diffractometer (XRD) using Cu Kα radiation, and the sample tank was made by SiO_2. The composites samples were polished and etched with Keller's reagent, then observed by the JSM-7500F field emission scanning electron microscope (SEM) equipped with an energy dispersive spectrometer (EDS). The average grain size of the samples was determined in

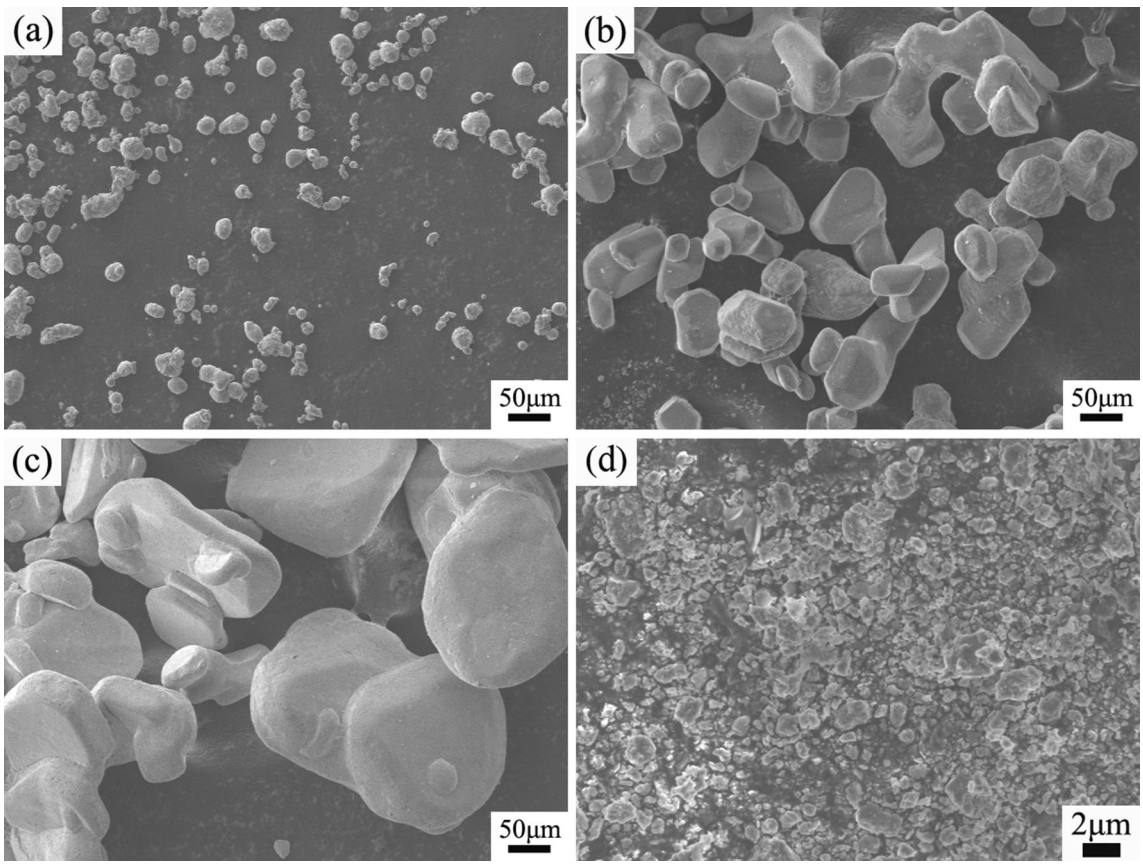

Fig. 1 SEM comparison of the powders before and after ball milling. (a) Al (b) KBF_4 (c) K_2TiF_6 (d) ball milled mixing powder

accordance with ASTM E112-2013 Standard using the Quantimet Image analysis method.

The reinforcement extraction experiments of the composites are as follows. The composites were placed on the anode, the copper plate was placed on the cathode, and the electrolyte was 3.3 mol/L KCl aqueous solutions. MD-30 pulse power with constant current mode was used to conduct the reinforcement extraction experiments. The anode slime of electrolysis experiment was cleaned and dried with dilute HCl solution and absolute ethanol to obtain the extractions.

T6 heat treatment, 530 °C for 6 h then water cooled, followed by 170 °C for 10 h then air cooled to room temperature, was carried to treat 6061 matrix and composites (Ref 31). HBS-3000 Brinell hardness tester was used to test the hardness of the samples, and the hardness value of the samples was the average value of five measurements. The tensile test was performed by an electronic universal tensile tester (CMT-5105, SANS) at room temperature with a crosshead velocity of 2 mm/min. The plate tensile specimens have a gage length of 21 mm and a thickness of 2 mm. MMU-10G wear test machine was used to test the wear properties of the composites under oil-lubricated conditions. GCr15 (45∼50 HRC) was used as disk with a roughness Ra = 0.8. The disk having diameter of 43 mm and 7 mm thickness was used in the present paper. The pin samples were prepared with the dimensions of 4 mm × 12 mm (diameter × length). The pin-disk wear tests were carried out with sliding speed of 200 rpm/min and 400 N constant loads for 30 min. SEA-40 lubricating oil was added 5 drops in every 10 min. The samples were cleaned in KQ2200DE ultrasonic cleaning machine with acetone solution before and after the experiment. The initial and final weight of the samples was measured with a precision of 0.0001 g in an electronic balance weighing machine. The wear rate of the samples is determined using the following expression:

$$A = \frac{W_1 - W_2}{S} \quad \text{(Eq 1)}$$

where W_1 is the weight of the sample before wear in mg, W_2 is the weight of the sample after wear in mg and S is the area of the wear surface of the sample in mm^2.

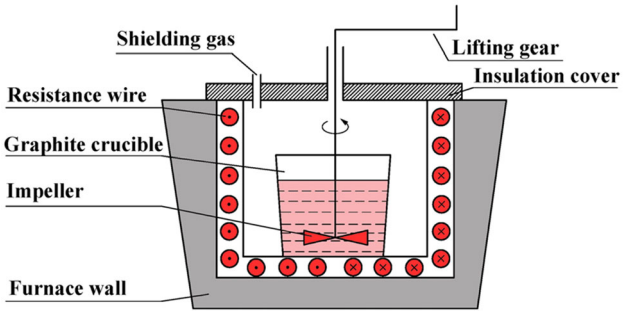

Fig. 2 Schematic illustration of the set-up for preparing in-situ TiB_2/6061 composites

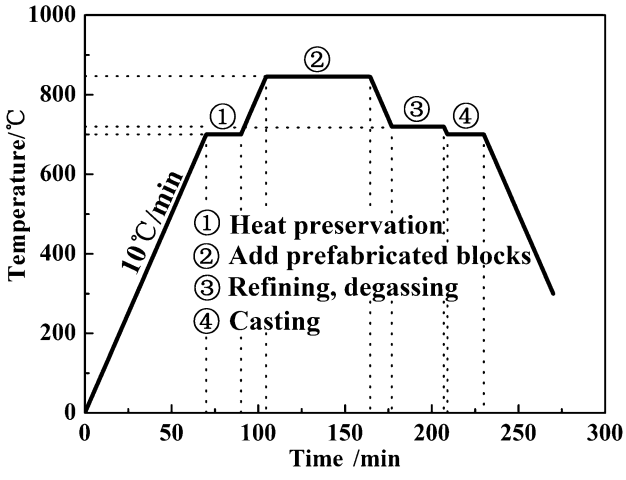

Fig. 3 Preparation process diagram of in-situ synthesized TiB_2/6061 composites

3. Results and Discussions

3.1 Phase identification

The reaction taken place in the Al-KBF_4-K_2TiF_6 system is as follow (Ref 32, 33):

$$K_2TiF_6 + KBF_4 + Al \rightarrow TiB_2 + KAlF_4 + KF + AlF \quad \text{(Eq 2)}$$

The main components in the reaction system are Al, Ti and B. Al is equivalent to the solvent; Ti and B are equivalent to the solutes. Therefore, the Eq 2 thermodynamic system can be regarded as Al-Ti-B system. The Eq 2 reaction can be described as follows:

$$3Al + [Ti] \rightarrow TiAl_3 \quad \text{(Eq 3)}$$

$$Al + 2[B] \rightarrow AlB_2 \quad \text{(Eq 4)}$$

$$[Ti] + [B] \rightarrow TiB \quad \text{(Eq 5)}$$

$$[Ti] + 2[B] \rightarrow TiB_2 \quad \text{(Eq 6)}$$

The standard Gibbs free-energy of the Al-Ti-B reaction system is calculated, as shown in Fig. 4. The Gibbs free-energy of Eq 6 is the lowest. As the reactions can be fully taken place, TiB_2 is the only stable phase, and the other products are all transformed to TiB_2.

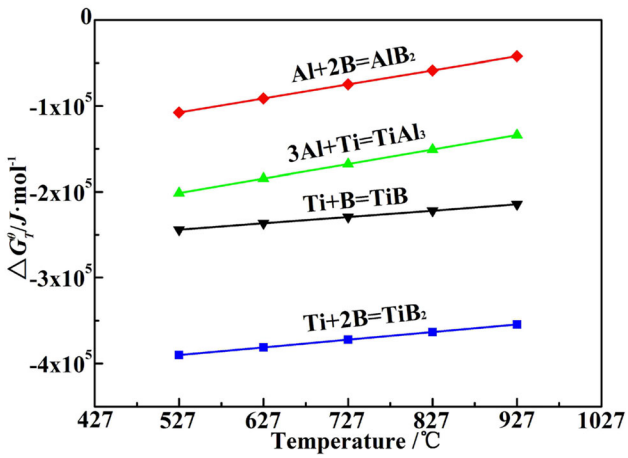

Fig. 4 The standard Gibbs free-energy of the Al-Ti-B system

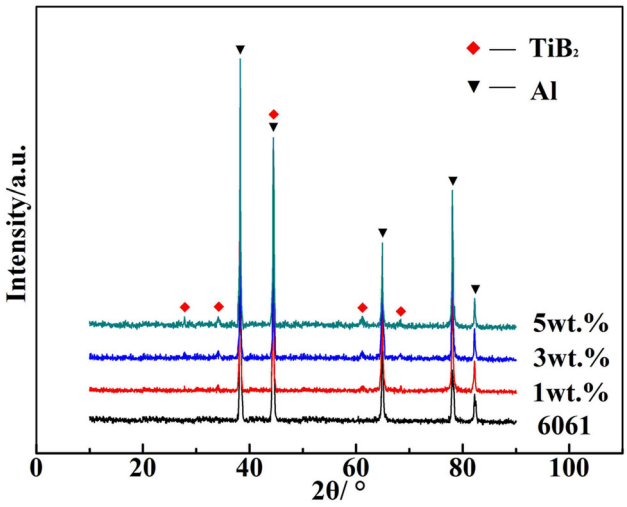

Fig. 5 DSC curve of mixed powder after ball milling

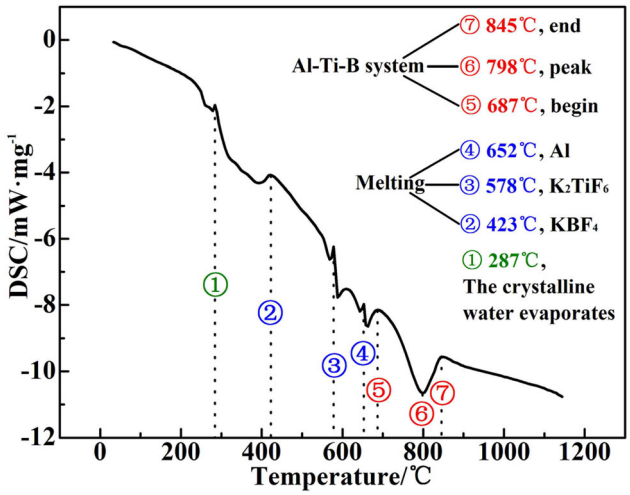

Fig. 6 X-ray diffraction patterns of in-situ synthesized TiB_2/6061 composites

Figure 5 is the DSC curve of mixed powder after ball milling. The exothermic of Al-Ti-B system start at 678 °C, peak at 798 °C and finish at 845 °C. That is to say the reactions can be taken place completely at 845 °C. The exothermic peak temperature and finish temperature are lower than the literatures, which reported the same reaction system (Ref 24, 26). This is because the ball milling treatment to the starting materials can significantly reduce the reaction temperature of the reaction system (Ref 27, 34).

Figure 6 is the x-ray diffraction patterns of in-situ synthesized TiB_2/6061 composites. The phase composition of the composites mainly consists of Al and TiB_2, while $TiAl_3$ and AlB_2 are not found. This agrees well with the calculation results of standard Gibbs free-energy of the reaction system, as shown in Fig. 4.

Figure 7 shows the x-ray diffraction patterns of the extracts taken from TiB_2/6061 composites. The diffraction peaks of TiB_2, Al_2O_3 and SiO_2 appear in the diffraction patterns. Al_2O_3 is the product of Al during extraction experiments, and the SiO_2 is the sample tank peak. Al and Mg_2Si, which dissolved in the

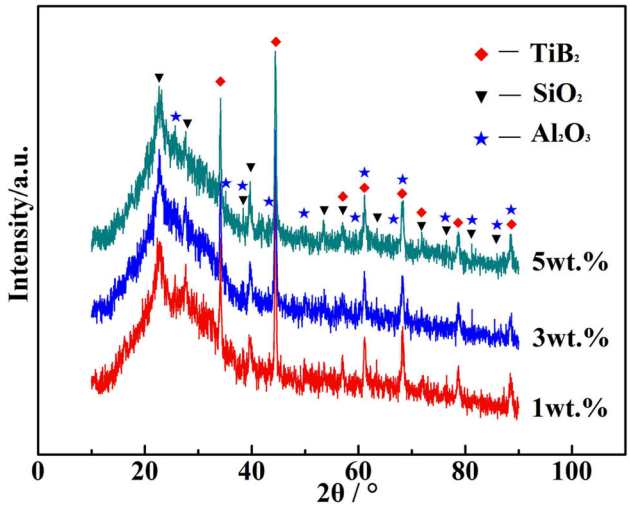

Fig. 7 X-ray diffraction patterns of the extracts taken from TiB_2/6061 composites

dilute HCl solution, are not found. TiB_2 is the only stable phase in the composites.

Figure 8 shows the SEM and EDS micrographs of the extracted TiB_2 taken from TiB_2/6061 composites. A large number of polygonal particles with the size distribution of 0.5∼1.5 μm can be seen from Fig. 8a. Figure 8(b)∼(f) are the results of the EDS analysis of the extracts. Ti and B elements are concentrated in the same position. Combined with Fig. 8(a), polygon particles are the main enrichment regions of Ti and B elements, and it can infer that polygonal particles in Fig. 8(a) are TiB_2 particles.

3.2 Microstructure Observation

Figure 9 shows SEM micrographs comparison of the matrix and TiB_2/6061 composites. It can be seen from Fig. 9(a) that the microstructure of 6061 aluminum matrix is composed of α(Al) + β(Mg_2Si) two-phase eutectic, and the second phase particle Mg_2Si is distributed at the grain boundary, and a small amount is distributed in the grain. The grain size of in-situ synthesized 1 wt.% TiB_2/6061 composites falls to 119.6 μm, reduced from the 154.7 μm in average size in 6061 aluminum matrix, as shown in Fig. 9(a) and (b). As the TiB_2 content increases to 3 wt.%, the grains are further refined with an average size of 74.8 μm, as shown in Fig. 9(c). However, compared with the 3 wt.% TiB_2/6061 composites, the grain size of the composites increases to 89.7 μm when the TiB_2 particle content increases to 5 wt.%, as shown in Fig. 9(d). This may due to the aggravated aggregation of reinforcing particles, which can reduce the grain refinement of the composites (Ref 35).

Figure 10 shows the SEM and EDS analysis of reinforcing particles in TiB_2/6061 composites. From Fig. 10(a)∼(c), polygonal particles with the size distribution of 0.5∼1.5 μm and the average size of 1 μm are dispersed in the matrix. The TiB_2 particles are distributed uniformly in the 1 wt.% TiB_2/6061 composites, as shown in Fig. 10(a). The TiB_2 particles agglomeration can be found in the 3 wt.% TiB_2/6061 composites, as shown in Fig. 10(b). As the particle content achieves 5 wt.%, serious particles agglomeration can be found in the composites, as shown in Fig. 10(c). Figure 10(d) is the point scan energy spectrum analysis results of the particles in

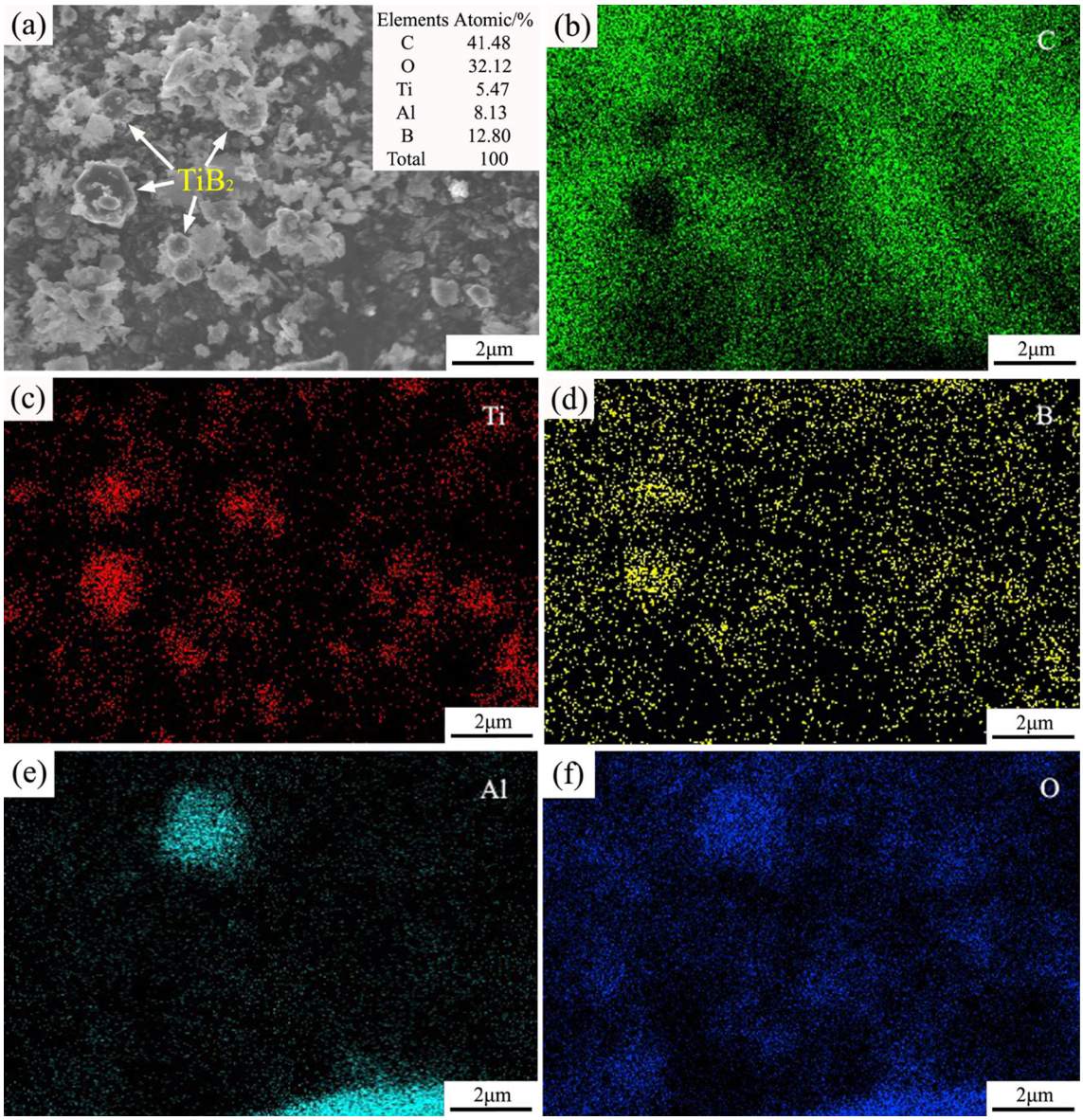

Fig. 8 SEM and EDS micrographs of extracted TiB_2 taken from TiB_2/6061 composites

Fig. 10(a)∼(c), and it can be seen that the multilateral particles only contain Al, Ti and B elements, so the polygonal particles in Fig. 11 are TiB_2 particles.

3.3 Hardness and Tensile Properties

The effect of TiB_2 particle content on the hardness of TiB_2/6061 composites is shown in Fig. 11. The hardness of 6061 aluminum matrix is 101.2 HBS after T6 heat treatment. With the increasing of TiB_2 particle content, the hardness of the composites increases first and then decreases. As the TiB_2 content is 3 wt.%, the hardness of the composites achieves the highest value (125.9 HBS), which is 24.4% higher than that of 6061 aluminum matrix. The hardness of the matrix and composites is better than those of the same materials reported in literature (Ref 17).

Figure 12 shows the effect of TiB_2 content on the tensile properties of TiB_2/6061 composites. The tensile properties of TiB_2/6061 composites are much higher than the matrix. With the increasing of TiB_2 content, the tensile strength, yield strength and Young's modulus of the composites first increase and then decrease. As the TiB_2 content achieves 3 wt.%, the tensile strength, yield strength and Young's modulus of the composites are the highest (308.9 MPa, 268.1 MPa and 84 GPa, respectively), which increase 16.2%, 15.9% and 23.5% compared with 6061 aluminum matrix, and their properties are better than those of the same materials reported in literature (Ref 18). The elongation of the composites decreased with the increasing of TiB_2 particle content; however, the decrement was not significant.

Figure 13 shows the SEM micrographs of fracture surface of the matrix and TiB_2/6061 composites. A number of deep equiaxed dimples were distributed in the fracture surface of 6061 aluminum matrix, as shown in Fig. 13(a), exhibiting a typical ductile failure. It can been seen in Fig. 13(b)∼(d), with the increasing of TiB_2 content, the dimples with reduced size were observed and the depth of the dimples decreased. This indicates that the ductility of TiB_2/6061 composites is lower than the matrix, which agrees well with elongation results in

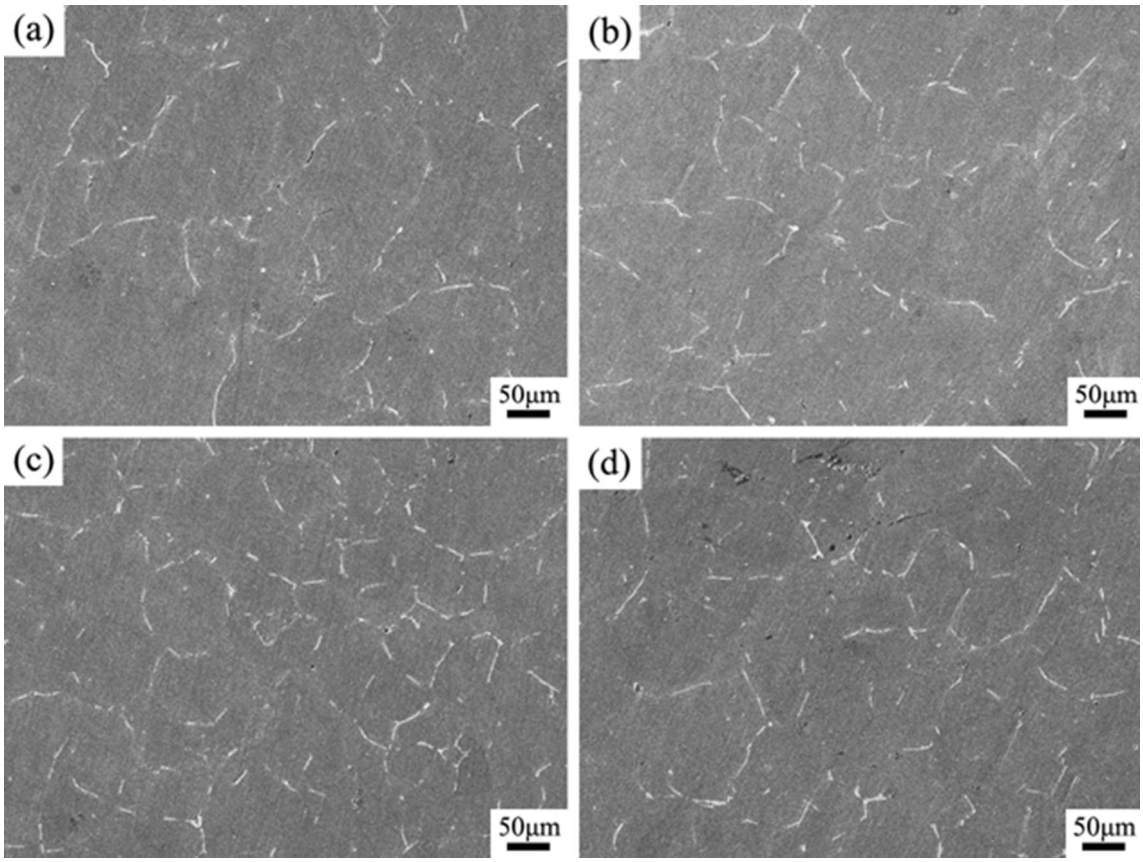

Fig. 9 SEM micrographs comparison of the matrix and TiB_2/6061 composites. (a) 6061, (b) 1 wt.% TiB_2/6061, (c) 3 wt.% TiB_2/6061 and (d) 5 wt.% TiB_2/6061

Fig. 13(a). Also, TiB_2 particles seriously agglomerate observed in the 5 wt.% TiB_2/6061 composites, as shown in Fig. 13(d). Under external load, the stress concentration occurs in the particles agglomeration regions and the cracks will initiate and propagate in agglomeration regions, resulting in the plasticity decreased, as shown in Fig. 12(a).

In general, the yield strength enhancement of particulate reinforced metal matrix composites can be estimated by two methods (Ref 36): load transferring and micromechanics strengthening mechanism. In the present paper, the TiB_2 volume fraction of the 1 wt.% TiB_2/6061, 3 wt.% TiB_2/6061 and 5 wt.% TiB_2/6061 are 0.006%, 0.018% and 0.031%, respectively. Because of the reinforcing particle volume fraction is quite lower than 5%, load transferring strengthening contribution to the yield strength enhancement is very small (Ref 37). The micromechanics strengthening mechanism includes grain refinement strengthening, Orwan strengthening and CTE strengthening. The quantitative contributions to the yield strength of the micromechanics mechanisms are discussed as follow.

(1) Grain refinement strengthening. Dislocation slip can be blocked by the grain boundaries to strengthen the matrix (Ref 36). The TiB_2 particles refine the grains of aluminum matrix, which providing more grain boundaries to hinder the dislocation motion. The contribution of grain refinement to the yield strength of the composites can be determined (Ref 37):

$$\Delta\sigma_{GR} = \beta D^{-1/2} \quad \text{(Eq 7)}$$

where β depends on a number of factors, and its typical value is 0.1 MPa·m$^{1/2}$, D is the average grain size of the composites.

(2) Orwan strengthening. The Young's modulus of the TiB_2 (530 GPa) is high enough to make the dislocation to loop around the TiB_2, which can make the plastic deformation of the composites more difficult. The yield strength contribution of Orwan strengthening can be calculated by the following expression (Ref 38):

$$\Delta\sigma_{OR} = \frac{2Gb}{d\left(\frac{\pi}{6V_p}\right)^{1/3}} \quad \text{(Eq 8)}$$

where G (26 GPa) and b (0.286 nm) are the shear modulus and Burgers vector of the matrix, d and V_p are the average diameter and volume fraction of the TiB_2 particles.

(3) CTE strengthening. The dislocation density can be increased owing to the difference of the coefficient of thermal expansion (CTE) between TiB_2 particles and the aluminum matrix. The yield strength enhancement by CTE strengthening can be calculated by the following expression (Ref 39):

$$\Delta\sigma_{CTE} = Gb\sqrt{\frac{12\Delta\alpha\Delta T V_p}{bd(1-V_p)}} \quad \text{(Eq 9)}$$

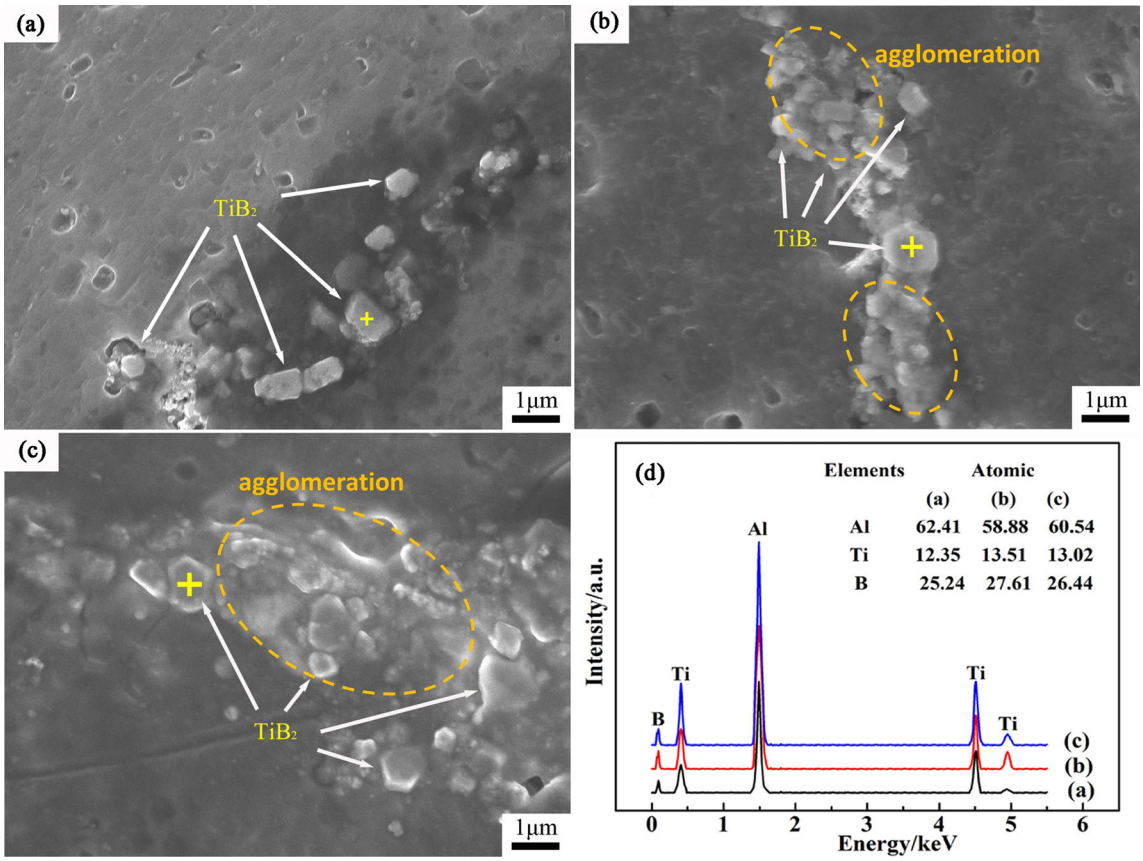

Fig. 10 SEM and EDS analysis of reinforcing particles in TiB_2/6061 composites. (a) 1 wt.%, (b) 3 wt.%, (c) 5 wt.%, (d) point energy spectrum analysis in (a), (b) and (c)

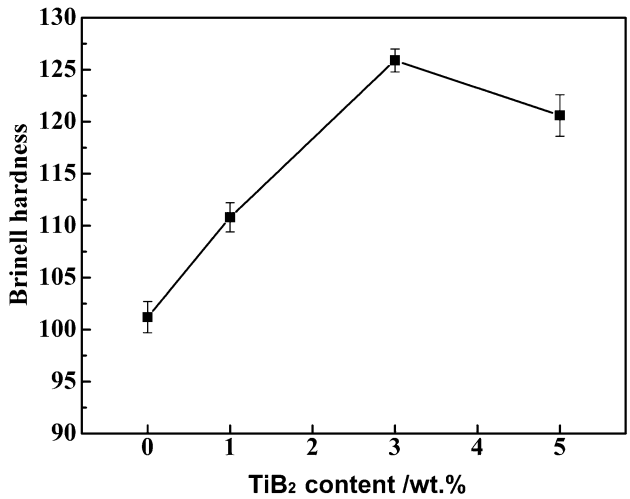

Fig. 11 The effect of TiB_2 content on the hardness of TiB_2/6061 composites

where $\triangle\alpha$ is the difference of the coefficient of thermal expansion between the matrix (23.6×10^{-6} K^{-1}) and TiB_2 (8.3×10^{-6} K^{-1}), $\triangle T$ is the difference between the processing temperature and test temperature. In this work, the molten temperature (700 °C) was taken as the processing temperature, and the temperature of the pre-heated mold (300 °C) was taken as the test temperature.

The total increment of yield strength due to the above three micromechanics mechanisms can be summarized as follows (Ref 37):

$$\Delta\sigma_{\text{Total}} = \Delta\sigma_{\text{GR}} + \sqrt[2]{\Delta\sigma_{\text{OR}}^2 + \Delta\sigma_{\text{CTE}}^2} \quad \text{(Eq 10)}$$

The calculated yield strength enhancement from different strengthening mechanisms is given in Table 1. For the 1 wt.% TiB_2/6061, the calculated yield strength enhancement of the composites is higher than the experiment values, which is possibly caused by low TiB_2 particles content. The calculated yield strength enhancement value for 3 wt.% TiB_2/6061 is 32.8 MPa, which is very close to the experiment value of 35.7 MPa. For the 5 wt.% TiB_2/6061, the calculated yield strength enhancement of the composites is much higher than the experiment values, which is probably caused by TiB_2 particles agglomerations and voids in the composites, as shown in Fig 10. Compared with the three mechanisms, it is evident that the CTE strengthening is the most effective one, followed by grain refinement strengthening and Orwan strengthening. Moreover, the CTE strengthening plays an important role as increasing the TiB_2 content.

3.4 Wear Resistance

Effect of TiB_2 content on the average friction coefficient and wear rate of TiB_2/6061 composites is shown in Fig. 14. The average friction coefficient and wear rate of TiB_2/6061 composites are lower than the matrix alloy. The formation of TiB_2 particles can improve the wear resistance of matrix. The

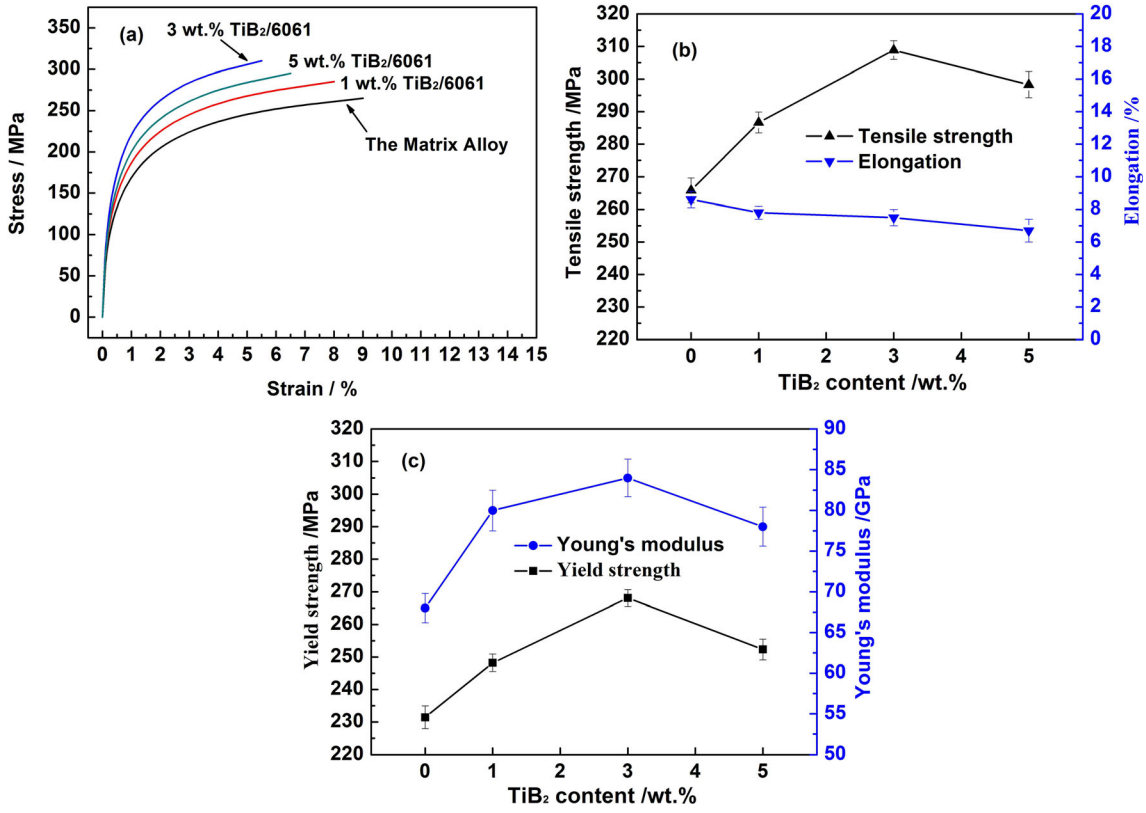

Fig. 12 Effect of TiB_2 content on the tensile properties of TiB_2/6061 composites. (a) Typical stress–strain curves, (b) average tensile strength and elongation, (c) average Young's modulus and yield strength

average friction coefficient and wear rate of TiB_2/6061 composites decrease first and then increase with the increasing of TiB_2 particle content. As the particle content achieves 3 wt.%, the average friction coefficient and wear rate of the composites are the lowest, which are 0.052 and 0.071 mg mm^{-2}, respectively, which decrease 22.4% and 26% compared with 6061 aluminum matrix.

Figure 15 shows the SEM and EDS analysis of worn surface of the matrix and TiB_2/6061 composites. A lot of grooves on the worn surface of 6061 and TiB_2/6061 composites can be seen from Fig. 15(a) to (d), which is affected by the abrasive wear mechanism. Compared with Fig. 15(a), the grooves on the worn surface of 1 wt.% TiB_2/6061 composites become thinner and shallower, as shown in Fig. 15(b). It is obvious that the grooves on the worn surface of 3 wt.% TiB_2/6061 composites are quite thin and shallow, which are difficultly observed, as shown in Fig. 15(c). However, the grooves appeared again on worn surface of 5 wt.% TiB_2/6061 composites. The EDS results show that the grooves contain TiB_2 particles and oxygen is not found, indicating oxidation of the friction surface does not occur.

In the present paper, the wear mechanism of in-situ TiB_2/6061 composites is abrasive wear. Base on the Archard wear theory, the abrasive wear can be described in Eq 12 (Ref 40).

$$v = \frac{k_{\mathrm{abr}} W x}{H} \qquad \text{(Eq 11)}$$

where v is the wear volume loss, W is the applied load, x is the sliding distance, H is the hardness of the worn surface, k_{abr} is a constant. The Eq 12 indicates that the higher hardness of the materials, the smaller wear loss. The 3 wt.% TiB_2/6061 composites have the highest hardness, which result in the best wear resistance as shown in Fig. 14. The lower wear resistance of 5 wt.% TiB_2/6061 composites attributes to the lower hardness compared with 3 wt.% TiB_2/6061 composites. On the other hand, serious TiB_2 particles agglomeration can be found in the 5 wt.% TiB_2/6061 composites, as shown in Fig. 10(c) can readily fall off because of higher brittleness during the wear process. The exfoliated hard particles would accelerated wear process, which also leads to the wear rate of the 5 wt.% TiB_2/6061 composites higher than that of 3 wt.% TiB_2/6061 composites. The lowest wear resistance of 1 wt.% TiB_2/6061 composites is because of the biggest grain size and the lowest hardness among these composites.

4. Conclusions

(1) In-situ synthesized TiB_2/6061 composites were prepared successfully from Al-K_2TiF_6-KBF_4 by high energy ball milling and stir casting. The average size of in-situ synthesized TiB_2 particles is 1 μm, which is polygonal shape. As the content of TiB_2 particles in the composites increases from 1 to 3 wt.%, the effect of grain refinement is remarkable. As the TiB_2 particles in the composites increase to 5 wt.%, the serious particles agglomerate happens, and reduces the grain refinement of the composites.

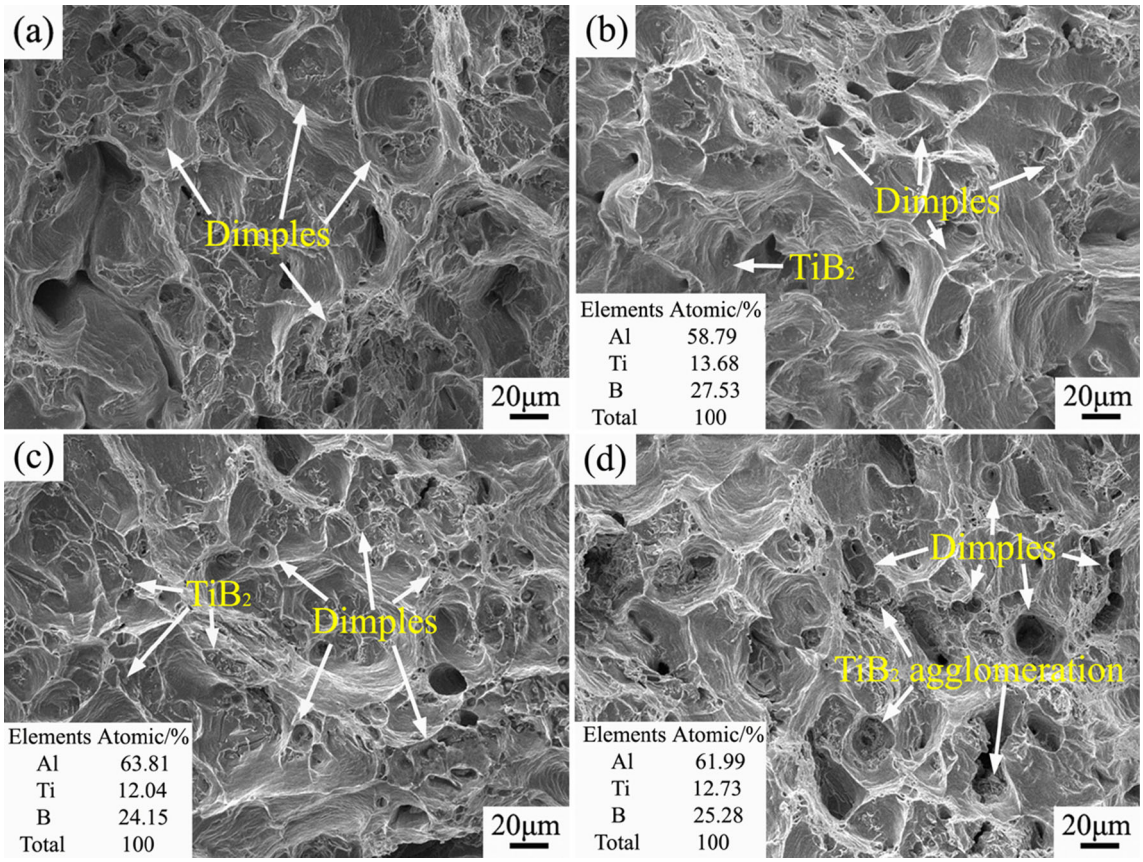

Fig. 13 SEM micrographs of fracture surface of the matrix and TiB_2/6061 composites. (a) 6061, (b) 1 wt.% TiB_2/6061, (c) 3 wt.% TiB_2/6061 and (d) 5 wt.% TiB_2/6061

Table 1 Calculated yield strength enhancement from different strengthening mechanisms (unit, MPa)

Materials	$\Delta\sigma_{GR}$	$\Delta\sigma_{OR}$	$\Delta\sigma_{CTE}$	$\Delta\sigma_{Total}$	$\Delta\sigma_{Experiment}$
1 wt.% TiB_2/6061	9.7	3.4	12	22.2	15.8
3 wt.% TiB_2/6061	11.5	4.7	20.8	32.8	35.7
5 wt.% TiB_2/6061	10.5	5.8	27.4	45.3	19.9

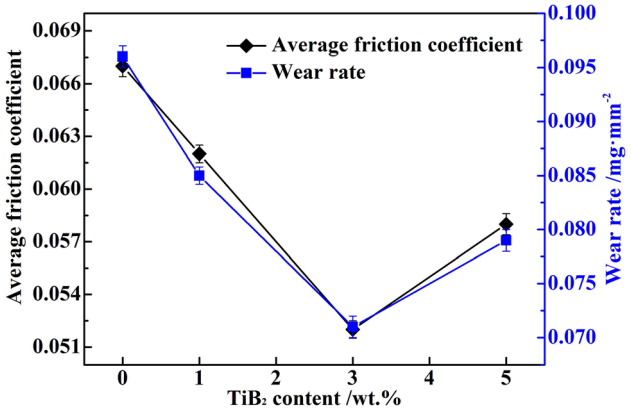

Fig. 14 Effect of TiB_2 content on the average friction coefficient and wear rate of TiB_2/6061 composites

(2) With the increasing of TiB_2 particles content from 1 to 5 wt.%, the hardness of the composites first increases and then decreases. As the content of TiB_2 particles is 3 wt.%, the hardness of the composites can achieve the highest value of 125.9 HBS, which is 24.4% higher than that of 6061 aluminum matrix.

(3) Tensile strength, yield strength and Young's modulus of the composites first increase and then decrease among the composites in ranges of the TiB_2 mass fraction from 1 to 5%. The elongation of the composites decreases with the increasing of TiB_2 particle content, but the decreasing is not obvious. Strengthening mechanisms of the TiB_2/6061 composites were fine grain strengthening, Orwan strengthening and CTE strengthening, in which the CTE strengthening plays an important role as increasing the TiB_2 content.

(4) Compared with the 1 wt.% and 5 wt.% TiB_2/6061 composites, 3 wt.% TiB_2/6061 composites have the highest hardness and best wear resistance. The average friction coefficient and wear rate are 0.052 and 0.071 mg mm^{-2},

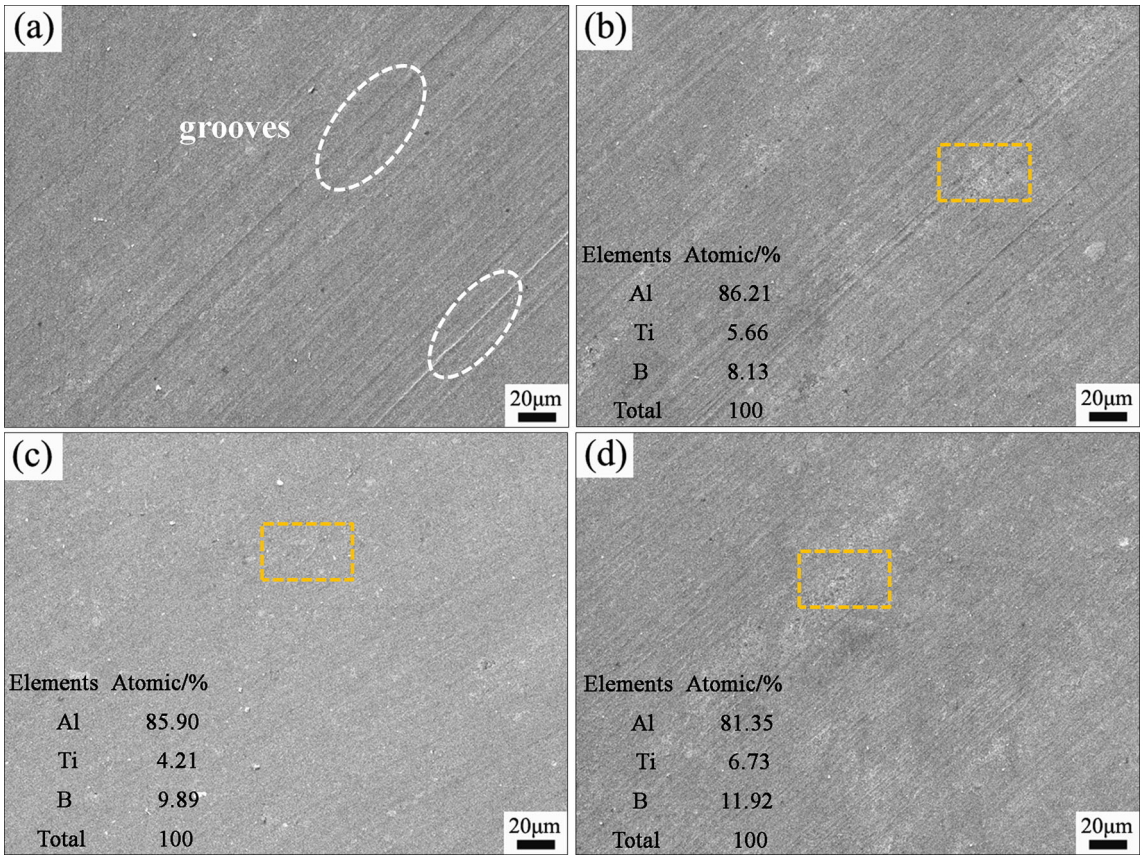

Fig. 15 SEM and EDS analysis of worn surface of the matrix and TiB_2/6061 composites. (a) 6061, (b) 1 wt.% TiB_2/6061, (c) 3 wt.% TiB_2/6061 and (d) 5 wt.% TiB_2/6061

respectively, which are 22.4% and 26% lower than 6061 aluminum matrix. The wear mechanism of TiB_2/6061 composites is abrasive wear.

Acknowledgments

This study was funded by National Natural Science Foundation for Youths (CN) (No. 51805235), Scientific Research Foundation of Educational Department of Liaoning Province for Basic Research (CN) (No. LJ2019JL008), Guidance Project of Natural Science Foundation of Liaoning Province (CN) (2019-ZD-0049), Discipline Innovation Team of Liaoning Technical University(LNTU20TD-18)and the PhD Research Startup Fund of Liaoning Technical University (CN) (No. 14-1034).

References

1. T.K. Ye, Y.X. Xu and J. Ren, Effects of SiC Particle Size on Mechanical Properties of SiC Particle Reinforced Aluminum Metal Matrix Composite, *Mat. Sci. Eng. A*, 2019, **753**, p 146–155
2. M. Cabeza, I. Feijoo, P. Merino, G. Pena, M.C. Pérez, S. Cruza and P. Rey, Effect of High Energy Ball Milling on the Morphology, Microstructure and Properties of Nano-Sized TiC Particle-Reinforced 6005A Aluminium Alloy Matrix Composite, *Powder. Technol.*, 2017, **321**, p 31–43
3. G.Q. Huang, J. Wu, W.T. Hou and Y.F. Shen, Microstructure, Mechanical Properties and Strengthening Mechanism of Titanium Particle Reinforced Aluminum Matrix Composites Produced by Submerged Friction Stir Processing, *Mat. Sci. Eng. A*, 2018, **734**, p 353–363
4. R.F. Liu, W.X. Wang, H.S. Chen, M.B. Tan and Y.Y. Zhang, Microstructure Evolution and Mechanical Properties of Micro-/Nano-Bimodal Size B_4C Particles Reinforced Aluminum Matrix Composites Prepared by SPS Followed by HER, *Vacuum*, 2018, **151**, p 39–50
5. V.G. Arigela, N.R. Palukuri, D. Singh, S.K. Kolli, J. Rengaswamy, P. Chekhonin, J. Scharnweber and W. Skrotzki, Evolution of Microstructure and Mechanical Properties in 2014 and 6063 Similar and Dissimilar Aluminium Alloy Laminates Produced by Accumulative Roll Bonding, *J. Alloy. Compd.*, 2019, **790**, p 917–927
6. P. Garg, A. Jamwal, D. Kumar, K.K. Sadasivuni, C.M. Hussain and P. Gupta, Advance Research Progresses in Aluminium Matrix Composites: Manufacturing and Applications, *J. Mater. Res. Technol.*, 2019, **8**(5), p 4924–4939
7. Z.N. Chen, T.M. Wang, Y.P. Zheng, Y.F. Zhao, H.J. Kang and L. Gao, Development of TiB_2 Reinforced Aluminum Foundry Alloy Based In Situ Composites – Part I: An Improved Halide Salt Route to Fabricate Al–5 wt.%TiB_2 Master Composite, *Mat. Sci. Eng. A*, 2014, **605**, p 301–309
8. M. Ao, H.M. Liu and C.F. Dong, The Effect of La_2O_3 Addition on Intermetallic-Free Aluminium Matrix Composites Reinforced with TiC and Al_2O_3 Ceramic Particles, *Ceram. Int.*, 2019, **45**(9), p 12001–12009
9. V. Chak, H. Chattopadhyay and T.L. Dora, A Review on fabrication Methods, Reinforcements and Mechanical Properties of Aluminum Matrix Composites, *J. Manuf. Process.*, 2020, **56**, p 1059–1074
10. N. Muralidharan, K. Chockalingam, I. Dinaharan and K. Kalaiselvan, MICROSTRUCTURE and Mechanical behavior of AA2024 Aluminum Matrix Composites Reinforced with In Situ Synthesized ZrB_2 Particles, *J. Alloy. Compd.*, 2018, **735**, p 2167–2174
11. S.A. Sajjadi, H.R. Ezatpour and H. Beygi, Microstructure and Mechanical Properties of Al–Al_2O_3 Micro and Nano Composites Fabricated by Stir Casting, *Mat. Sci. Eng. A*, 2011, **528**(29), p 8765–8771

12. P. Samal, P.R. Vundavilli, A. Meher and M.M. Mahapatra, Recent Progress in Aluminum Metal matrix Composites: A Review on Processing, Mechanical and Wear Properties, *J. Manuf. Process*, 2020, **59**, p 131–152
13. K. Sinan, Effects of TiB_2 Nanoparticle Content on the Microstructure and Mechanical Properties of Aluminum Matrix Nanocomposites, *Mater Test*, 2017, **59**(10), p 844–852
14. A.R. Najarian, R. Emadi and M. Hamzeh, Fabrication of as-Cast Al Matrix Composite Reinforced by Al_2O_3/Al_3Ni Hybrid Particles Via in-Situ Reaction and Evaluation of its Mechanical Properties, *Mat. Sci. Eng. B*, 2018, **231**, p 57–65
15. Y. Afkham, R.A. Khosroshahi, S. Rahimpour, C. Aavani, D. Brabazon and R.T. Mousavian, Enhanced Mechanical Properties of In Situ Aluminium Matrix Composites Reinforced by Alumina Nanoparticles, *Arch. Civ. Mech. Eng.*, 2018, **18**(1), p 215–226
16. K.N. Mathan and K.L. Annamalai, Characterization and Tribological analysis on AA 6061 Reinforced with AlN and Zrb_2 In Situ Composites, *J. Mater. Res. Technol.*, 2019, **8**(1), p 969–980
17. C.S. Ramesh, S. Pramod and R. Keshavamurthy, A Study on Microstructure and Mechanical Properties of Al 6061–TiB_2 In-Situ Composites, *Mat. Sci. Eng. A*, 2011, **528**(12), p 4125–4132
18. Y. Pazhouhanfar and B. Eghbali, Microstructural Characterization and Mechanical Properties of TiB_2 Reinforced Al6061 Matrix Composites Produced Using Stir Casting Process, *Mat. Sci. Eng. A*, 2018, **710**, p 172–180
19. J. Zhang, D. Zhang, H. Zhu and Z. Xie, In-Situ TiC Reinforced Al-4Cu Matrix Composite: Processing, Microstructure and Mechanical Properties, *Mat. Sci. Eng. A*, 2020, **794**, p 139946
20. H. Yang, T. Gao, Y. Wu, H. Zhang, J. Nie and X. Liu, Microstructure and Mechanical Properties at Both Room and High Temperature of In-Situ TiC Reinforced Al–4.5Cu Matrix Nanocomposite, *J. Alloy. Compd.*, 2018, **767**, p 606–616
21. T. Gao, L. Liu, J. Song, G. Liu and X. Liu, Synthesis and Characterization of an In-Situ Al_2O_3/Al–Cu Composite with a Heterogeneous Structure, *J. Alloy. Compd.*, 2021, **868**, p 159283
22. S. Lei, X.F. Li, Y.Q. Deng, Y.K. Xiao, Y.C. Chen and H.W. Wang, Microstructure and Mechanical Properties of Electron Beam Freeform Fabricated TiB_2/Al-Cu Composite, *Mater. Lett.*, 2020, **277**, p 128273
23. X.X. Dong, H. Youssef, Y.J. Zhang, H.L. Yang, S.H. Wang and S.X. Ji, Advanced Heat Treated Die-Cast Aluminium Composites Fabricated by TiB_2 Nanoparticle Implantation, *Mater. Des.*, 2019, **186**, p 108372
24. J. Liu, Z.W. Liu, Z.W. Dong, X.L. Cheng, Q.L. Zheng, J. Li, Z. Sha, Z.F. Huang, Y.M. Gao, J.D. Xing and Q.Y. Han, On the Preparation and Mechanical Properties of In Situ Small-Sized TiB_2/Al-4.5Cu Composites Via Ultrasound Assisted RD Method, *J. Alloy. Compd.*, 2018, **765**, p 1008–1017
25. S. Mozammil, J. Karloopia, R. Verma and P.K. Jha, Effect of Varying TiB_2 Reinforcement and its Ageing Behaviour on Tensile and Hardness Properties of In-Situ Al-4.5%Cu-xTiB_2 Composite, *J. Alloy. Compd.*, 2019, **793**, p 454–466
26. F. Chen, Z. Chen, F. Mao, T. Wang and Z. Cao, TiB_2 Reinforced Aluminum Based In Situ Composites Fabricated by Stir Casting, *Mat. Sci. Eng. A*, 2015, **625**, p 357–368
27. S.L. Zhang, J. Yang, B.R. Zhang, Y.T. Zhao, G. Chen, X.X. Shi and Z.P. Liang, A Novel Fabrication Technology of In Situ TiB_2/6063Al Composites: High Energy Ball Milling and Melt In Situ Reaction, *J. Alloy. Compd.*, 2015, **639**, p 215–223
28. L. Lü, M.O. Lai, Y. Su, H.L. Teo and C.F. Feng, In Situ TiB_2 Reinforced Al Alloy Composites, *Scripta Mater.*, 2001, **45**(9), p 1017–1023
29. K.L. Tee, L. Lu and M.O. Lai, Synthesis of In Situ Al-TiB_2 Composites Using Stir Cast Route, *Compos. Struct.*, 1999, **47**(1–4), p 589–593
30. J.V. Wood, D.G. McCartney, K. Dinsdale, J.L.F. Kellie and P. Davies, Casting and Mechanical Properties of a Reactively Cast Al-TiB_2 Alloy, *Cast Metal.*, 1995, **8**(1), p 57–64
31. J. Yi, G. Wang, S.K. Li, Z.W. Liu and Y.L. Gong, Effect of Post-Weld Heat Treatment on Microstructure and Mechanical Properties of Welded Joints of 6061–T6 Aluminum Alloy, *T. Nonferr. Metal. Soc.*, 2019, **29**(10), p 2035–2046
32. S. Agrawal, A.K. Ghose and I. Chakrabarty, Effect of Rotary Electromagnetic Stirring During Solidification of In-Situ Al-TiB_2 Composites, *Mater. Design.*, 2017, **113**, p 195–206
33. A. Kumar, R.K. Gautam and R. Tyagi, Dry Sliding Wear characteristics of In Situ Synthesized Al-Tic Composites, *Compos. Interface.*, 2016, **23**(6), p 469–480
34. Z.Y. Yu, N.Q. Zhao, E.Z. Liu, C.S. Shi, X.W. Du and J. Wang, Low-Temperature Synthesis of Aluminum Borate Nanowhiskers on the Surface of Aluminum Powder Promoted by Ball-Milling Pretreatment, *Powder. Technol.*, 2011, **212**(2), p 310–315
35. R. Raghu, J. Nampoothiri and T.S. Kumar, In-Situ Generation of $MgAl_2O_4$ Particles in Al-Mg Alloy Using H_3BO_3 Addition for Grain Refinement Under Ultrasonic Treatment, *Measurement*, 2018, **129**, p 389–394
36. I.S. Lee, C. Hsu, C.F. Chen, N.J. Ho and P.W. Kao, Particle-Reinforced Aluminum Matrix Composites Produced from Powder Mixtures Via Friction Stir Processing, *Compos. Sci. Technol.*, 2011, **71**(5), p 693–698
37. T.W. Clyne and P.J. Withers, *An Introduction to Metal Matrix Composites*, 1st ed. Cambridge University Press, Cambridge, 1993
38. S. Jayalakshmi, S. Gupta, S. Sankaranarayanan, S. Sahu and M. Gupta, Structural and Mechanical Properties of Ni60Nb40 Amorphous Alloy Particle Reinforced Al-Based composites Produced by Microwave-Assisted Rapid Sintering, *Mat. Sci. Eng. A*, 2013, **581**, p 119–127
39. G. Huang, J. Wu, W. Hou and Y. Shen, Microstructure, Mechanical Properties and Strengthening Mechanism of Titanium Particle Reinforced Aluminum Matrix Composites Produced by Submerged Friction Stir Processing, *Mat. Sci. Eng. A*, 2018, **734**, p 353–363
40. B. Bhushan, *Introduction to Tribology*, 2nd ed. Wiley, Chichester, 2013